SI Appendix comprises: Supplemental Results and Discussion, Supplemental Table 1, Supplemental Methods, Supplemental Figures S1-S7, Supplemental Video Legends and Supplemental References

Supplemental Results and Discussion

Cooperation between WSP-1/N-WASP and WVE-1/WAVE is consistent with RhoGTPase epistasis

Cooperation between the two Arp2/3 complex activators should be reflected in the upstream pathways involving the RhoGTPases that regulate WSP-1/N-WASP and WVE-1/WAVE function. In cell motility events in *C. elegans*, WSP-1/N-WASP is activated by both CDC-42/Cdc-42 and MIG-2/Rac, a Rac protein that contains Cdc42-like motifs, while WVE-1/WAVE is activated by CED-10/Rac (1-6).

Interfering with RhoGTPases individually gave the following effects: homozygous *cdc-42* and *ced-10* mutant worms isolated from heterozygous mothers and further treated with RNAi to eliminate possible maternal contribution displayed 68% and 97% invasion at the P6.p 4-cell stage, respectively, while *mig-2* mutant worms had no invasion defects (Supplemental Figure S6a). RNAi against *cdc-42* or *mig-2* in *wsp-1(gm324)* animals gave no additional reduction below the 18% invasion already observed after loss of *wsp-1* alone, suggesting that CDC-42 and MIG-2 were in the same pathway as WSP-1/N-WASP. However when *ced-10* was knocked down in *wsp-1(gm324)* animals, full invasion was reduced to 5%, similar to the invasion defect obtained with RNAi against *wve-1* in *wsp-1(gm324)* animals (Supplemental Figure S6a, see also Supplemental Table 1). Conversely when *ced-10* was knocked down in *wve-1* mutant animals, there was almost no defect in invasion at the P6.p 4-cell stage (96% full invasion), similar to loss of *wve-1* alone (Supplemental Figure S6a). When the WSP-1/N-WASP regulators *mig-2* and *cdc-42* were knocked down separately in the *wve-1* null background, there was little defect in invasion (90% and 81% full invasion, respectively), indicating that either one sufficed for WSP-1/N-WASP activation for invasion. Supporting this idea, when *cdc-42* was knocked down in animals mutant in *mig-2(mu28),* only 21% showed full invasion, similar to what was observed with the *wsp-1(gm324)* N-WASP-deleted worms (Supplemental Figure S6a). Compromising *mig-2* and *ced-10* together gave a less severe reduction in invasion (58% full invasion).

www.pnas.org/cgi/doi/10.1073/pnas.1808760115

All together these results supported the idea that WSP-1/N-WASP, downstream of CDC-42/Cdc-42, was the principal pathway by which the Arp2/3 complex was activated in the AC (left-most branch Supplemental Figure S6b). Nevertheless MIG-2/Rac could assure almost WT levels of invasion in the absence of CDC-42/Cdc-42. Parallel to this pathway, WVE-1/WAVE, activated by CED-10/Rac, appeared able to drive invasion in the absence of the CDC-42/Cdc-42-MIG-2/Rac-WSP-1/N-WASP activation pathways (right-most branch Supplemental Figure S6b). Taken together, the results with RhoGTPases further supported the idea that there were two independent pathways for activating the Arp2/3 complex during AC invasion, one via WSP-1/N-WASP and the other via WVE-1/WAVE, with the WSP-1/N-WASP axis playing the major role.

Supplemental Table S1. Genetic analysis of actin-binding proteins in AC invasion at the P6.p 4-cell stage

Genotype/treatment	Mammalian homologues [a]	% Full invasion	% Partial invasion	% No invasion	N
Arp2/3 complex RNAi					
arx-2 RNAi [b]	Arp2 (actin-related protein 2)	54	0	46	41
control L4440 RNAi [b]		100	0	0	35
Arp23/ complex inhibition (VCA expression in AC)					
curIs20 [Pzmp-1-pes10::TagBFP:: VCA(WASP)]		0	0	100	30
WASP/WAVE deletion/RNAi					
wsp-1 (gm324) [c]	N-WASP	18	28	54	50
wsp-1 (gm324); qyIs127[Plam-1::laminin::mCherry]; qyIs242 [Pcdh-3::Lifeact::GFP] [d]		18*	21	61	34
wsp-1 (gm324); qyIs127[Plam-1::laminin::mCherry]; qyIs242 [Pcdh-3::Lifeact::GFP] + wve-1 RNAi		5*	17	78	60
wve-1 (ne350) [e] *+ wve-1 RNAi* [f]	WAVE	94	3	3	35
Formin deletion/RNAi					
frl-1 (ok460)	FMNL1-3	98	0	2	52
fhod-1 (tm2363)	FHOD1 and 3	98	2	0	44
cyk-1 (ok2300)	DIA1-3	100	0	0	38
daam-1 (tm2133)	DAAM1 and 2	100	0	0	39
inft-2 (ok1296)	INF1	98	2	0	55
exc-6 (rh103) [g]	INF2	100	0	0	61
exc-6 (rh103) + cyk-1 RNAi		98	2	0	41
cyk-1 (or596ts); inft-2 (ok1296); exc-6 (gk386)		94	4	2	49
Crosslinker deletion/RNAi					
atn-1 (ok84)	α-actinin	100	0	0	39
plst-1 (tm4255)	plastin/fimbrin	100	0	0	39
fln-1 (tm545)	filamin	91	7	2	43
atn-1(ok84); plst-1(tm4255) + fln-1 RNAi [h]		95	5	0	41

[a] As described in (7-11).

[b] Performed in *qyIs127[Plam-1::laminin::mCherry]; qyIs242 [Pcdh-3::Lifeact::GFP]* worms.

[c] Data from (12) to compare to [d]. *wsp-1(gm324)* is reported to be a complete null (13).

[d] The same strain as in [c], but bearing Lifeact and labeled BM. The similarity indicates that the fluorescent labeling, including the use of Lifeact, is not perturbing dynamics in the AC.

[e] *wve-1(ne350)* is a functional null mutation in the WVE-1 protein (5).

[f] See Supplemental Methods for how worms were prepared for this experiment.

[g] The formin gene *exc-6* is strongly and specifically expressed in the AC (14).

[h] These worms suffered from low brood size, typical of worms lacking *fln-1* (15), indicating that the RNAi was effective.

* Statistical comparison showed a significant difference $p = 0.04$.

Supplemental Methods

Worm strains

OX308 strain carrying *wve-1(ne350)* I/hT2[*bli-4(e937) let-?(q782) qIs48*](I;III) was a gift of Martha Soto (Rutgers University). The triple formin mutant GS7960 *cyk-1(or596ts); exc-6(gk386); inft-2(ok1296)*; *arIs198* was a gift from Daniel Shaye (University of Illinois at Chicago) (16). CRISPR fluorescently-labeled endogenous *wsp-1* and *wve-1*, strain GOU2062 *cas762*[*TagRFP::wve-1a* knock-in] I; *cas723*[*GFP::wsp-1a* knock-in] IV was a gift from Guangshuo Ou (Tsinghua University) (17). The following strains were provided by the Caenorhabditis Genetics Center, which is funded by NIH Office of Research Infrastructure Programs (P40 OD010440): NG324 *wsp-1(gm324)* IV, DP38 *unc-119(ed3)* III, CF162 *mig-2(mu28)* X, LE1012 *ced-10(tm597)/dpy-13(e184)* IV, VC898 *cdc-42(gk388)*/mIn1 [mIs14 *dpy-10(e128)*] II, *frl-1* RB696 *Y48G9A.4(ok460)* III, VC1895 *cyk-1(ok2300)*/mT1 [*dpy-10(e128)*] III, *inft-2* RB1280 *F15B9.4(ok1296)* V/nT1 [qIs51] (IV;V), NJ833 *exc-6* (a.k.a. *inft-1*) *(rh103)* III, RB1812 *atn-1(ok84)* V. The National BioResource Project provided the following mutants: *fhod-1(tm2363)* I, *daam-1(tm2133)* V, *plst-1(tm4255)* IV, *fln-1 (tm545)* IV. Other strains used from previous studies were: NK389 *qyIs67* [*Pcdh-3::UNC-40::GFP + unc-119(+)*] (18), NK1588 *qyIs108* [*Plam-1::lam-1::dendra + unc-119(+)*]; *qyIs23* [*Pcdh-3::mCherry∷ PLCδPH + unc-119(+)*] (19, 20), NK1123 *qyEx260* [*Pzmp-1::GFP::ZMP-1-GPI*] (21). For assessing HIM-4/hemicentin secretion, the worm genotype was *rhIs23 [Phim-4::him-4::GFP]; qyIs50 [Pcdh-3::mCherry::moeABP]; rol-6(su1009)* (20). The alleles *syIs115(SPARC::GFP, unc-119(+))* and *syIs113(SPARC::GFP, unc-119(+))* were used interchangeably for the SPARC overexpression experiments (22).

The following strains were generated in the present study: JUP60 (NK696 crossed with NK1073) *unc-119(ed4)* III; *qyIs127 [Plam-1::lam-1::mCherry + unc-119(+)*]; *qyIs242* [*Pcdh-3::Lifeact::GFP + unc-119(+)*] (see also (18, 20)), JUP75 (NG324 crossed with JUP60) *wsp-1(gm324)* IV; *unc-119(ed4)* III; *qyIs127* [*Plam-1::lam-1::mCherry + unc-119(+)*]; *qyIs242* [*Pcdh-3::Lifeact::GFP + unc-119(+)*], JUP64 *unc-119(ed3)* III; *curIs20* [*Pzmp-1-pes10::TagBFP::VCA(WASP) + unc-119(+)*], JUP84 (JUP64 injected with Lifeact-GFP) *unc-119(ed3)* III; *curIs20* [*Pzmp-1-pes10::TagBFP::VCA(WASP) + unc-119(+)*]; *curEx21* [*Pcdh-3 ::Lifeact::GFP + Pmyo2::mCherry*], JUP83 (GOU2062 injected with Lifeact-BFP) *cas762*[*TagRFP::wve-1a* knock-in] I; *cas723*[*GFP::wsp-1a* knock-in] IV; *curEx22* [*Pcdh-3::Lifeact::tagBFP + Pmyo-2::mCherry*], JUP80 (RB1812 crossed with *plst-1*

(tm4255)) *atn-1(ok84)* V; *plst-1(tm4255)* IV, JUP72 *unc-119(ed3)* III; *curIs23* [*Pcdh-3::Lifeact::Dronpa-M159T + unc-119(+)*], JUP92 (NK1123 injected with BFP-VCA(WASP)) *qyEx260* [*Pzmp-1::GFP::ZMP-1-GPI*]; *curEx32 [Pzmp-1-pes10::TagBFP::VCA(WASP) + Pmyo2::mCherry*], and JUP93 *qyEx260* [*Pzmp-1::GFP::ZMP-1-GPI*]; *curEx33 [Pzmp-1-pes10::TagBFP::VCA(WASP) + Pmyo2::mCherry*].

The VCA-BFP and Lifeact-Dronpa strains were prepared by microinjection in DP38 *unc-119(ed3)* III, followed by integration using a UV Stratalinker. No coinjection marker was used as the *unc-119* rescue gene was in the backbone of the target plasmid. All injections in this study were performed with 1kb ladder to bring the total DNA concentration up to 100 ng/μL, with about 30 ng/μL target DNA except for the *Pmyo2::mCherry* marker (plasmid pCFJ90), which was injected at 2.5 ng/μL.

Plasmids and constructions

The dominant negative VCA construct (for *curIs20)* was prepared by amplifying VCA from a *wsp-1a* cDNA clone, yk184g1 (gift of Yuji Kohara, National Institute of Genetics, Mishima, Japan). The VCA fragment started at Gly485 and went to the stop codon. BFP was fused with VCA as an N-terminal tag and then recombined into Gateway cloning vector pDONR221. The promoter sequence *Pzmp-1* and the enhancer element *pes-10* were amplified from pBS-zmp-1p-pes-10-spGFP1-10 as done in (23), and introduced into Gateway cloning vector pDONR[P4-P1R]. The entry vectors were recombined along with the *unc-54 3'UTR* (gift of G. Seydoux; Addgene plasmid #17253: pCM5.37) into the destination vector pCFJ150 - pDESTttTi5605[R4-R3] (gift from Erik Jorgensen Addgene plasmid # 19329). For the Lifeact::GFP construct (for *curEx21*), the *cdh-3* promoter was amplified as in (20) and introduced into Gateway cloning vector pDONR[P4-P1R]. pENTR[1,2]Lifeact::GFP was from (24). The fragments were recombined as above with *unc-54 3'UTR* and pCFJ150. The Lifeact::BFP construct (for *curEx22*) was obtained the same way, except that Lifeact was first fused to tagBFP and introduced into pDONR221. For the Lifeact::Dronpa construct (*curIs23*), Lifeact and a linker as in (24) was synthesized in frame with DronpaM159T. The M159T variant is a faster switcher than the original Dronpa (25). The Dronpa sequence was obtained from the mammalian protein sequence by adapting it for *C. elegans* codon usage and putting in syntrons using the codon adapter developed in (26). The gene was synthesized by Eurofins Genomics.

Evaluating mutants and RNA interference

Mutant worms were synchronized by bleach to the L1 stage and then fed OP50 at 20°C until AC invasion was scored. RNAi was performed by feeding bacteria producing target dsRNAs to larvae. All larvae were bleach-synchronized L1s, except for *wsp-1* RNAi in polarity (UNC-40-GFP), trafficking (PH-mCherry and GFP-ZMP-GPI) and secretion (HIM-4-GFP) experiments, where L4s were fed and their progeny evaluated in order to produce a stronger RNAi effect. Phenotypes were scored at the 4-cell stage, except for HIM-4-GFP, which was observed ventrally by use of the *rol-6(su1009)* transgene at the 2-cell stage in order to better visualize HIM-4 puncta as in (27). Empty L4440 was used as a negative control. Probes were obtained from the Vidal ORF RNAi library (28), except for *fln-1* that was from the Ahringer RNAi collection (Source BioScience), *cyk*-1, *wsp*-1 and *arx-2* that were prepared from yk clones (Yuji Kohara, National Institute of Genetics, Mishima, Japan) and *wve-1* that was prepared from the ORF (ThermoScientific).

For the temperature sensitive *cyk-1* mutant (*or596ts*), worms were propagated at 15°C. Adult worms were allowed to lay eggs for 12h at 15°C, then adults were removed and embryos were switched to the restrictive temperature of 25°C until AC scoring. The WVE-1/WAVE mutation is embryonic lethal. Thus, homozygous *wve-1(ne350)* animals were isolated from heterozygous mothers for analysis, and were further treated with RNAi targeting *wve-1* to eliminate possible maternally contributed *wve-1* RNA. Confirming that these animals were completely lacking WVE-1/WAVE, they produced mostly dead eggs (the mothers had some maternally-inherited WVE-1/WAVE and thus made it through embryogenesis, but the progeny of homozygous null worms did not).

CK666 treatment

CK666 was purchased from Calbiochem/Merck. Synchronized larvae were allowed to develop to the late P6.p 1-cell/early 2-cell stage. 500 μL of 20 mM CK666 in water (or the equivalent of DMSO) was added directly to the worms on plates containing 10 mL of agar, and allowed to soak in, to give a final concentration of 1 mM CK666. Worms were examined 1-4 hours after CK666 addition. The drug blocked development and resulted in worm death over time. Incubating worms directly in 1 mM CK666 in liquid culture with OP50 food did not affect development or invasion so solid support and/or the initial high concentration of CK666 upon application to the agar gel must be important for drug uptake.

Imaging

Worms were anesthetized in 100 μL of 0.02% levamisole for about 15 min, and then mounted on 4.5% noble agar pads. Samples were sealed with melted VALAP (vaseline, lanolin, paraffin 1:1:1 w/w/w), leaving windows for oxygen exchange, and incubated in a humid chamber until imaged (29). Image acquisition was performed at 20°C. Coupled DIC and epifluorescence microscopy were performed on an Olympus BX51 upright microscope with a 100× oil immersion objective and Retiga R3 Monochrome CCD Camera (Roper Scientific). Spinning disk confocal fluorescence images were acquired on a Roper/Nikon inverted spinning disk confocal microscope, equipped with a CoolSnap HQ2 camera and a 100x/1.4 OIL DIC N2 PL APO VC objective. Paired DIC/spinning disc fluorescent images were taken on a Roper/Zeiss upright spinning disk confocal microscope, equipped with a CoolSnap HQ2 camera and a 100x/1.46 OIL DIC ALPHA PL APO (UV) VIS-IR objective. Both microscopes had 405, 491 nm and 561 nm laser lines and were controlled by Metamorph (Molecular Devices). Z-stacks were acquired at 30-90 s intervals with 0.5-μm distance between planes.

Image analysis

Indentations and angles were measured on DIC images in Metamorph of ImageJ. Actin area and density at the invasive front was quantified by thresholding and automatic detection of the bright actin patch in Metamorph. Area and total fluorescence intensity minus background were logged, and the latter divided by the former to obtain density values.

For colocalization analysis of GFP-WSP-1 and RFP-WVE-1, single plane images were background adjusted then merged. 15 pixel wide lines were drawn along AC invasive membrane and extended into low fluorescent regions on either side of the AC. Maximum intensities along the line were logged in each channel. Linescans were plotted and smoothed in Kaleidegraph. For correlation coefficients, the intensity of each pixel in the red channel was plotted as a function of its intensity in the green channel. The scatter plots were fit with a line to give the correlation coefficient.

For area and shape change quantification over time, maximum intensity projections were obtained over about 10 μm (20 slices), cropped and rotated, and then aligned to correct for worm movement using the Align function of Metamorph. Images were thresholded and protrusion areas were detected automatically. Unshared area between consecutive frames was

calculated using either the XOR tool of ROI Manager in Image J or a home-made macro. Curves of area and shape change increase over time were smoothed in Kaleidegraph.

Polarity measurements for UNC-40-GFP were performed on a single plane, dividing the mean intensity of the invasive membrane by the mean intensity of the apical and lateral membranes quantified using 5-pixel wide lines. % fluorescence at the invasive membrane for GFP-ZMP-1-GPI and PLCδ PH-mCherry was obtained using maximum intensity projections to maximize the visibility of cytoplasmic signal, and measuring the fluorescent signal found in the region along the AC invasive membrane versus the fluorescence in the rest of the cell. Background was subtracted from both. The data was represented as %: % = integrated fluorescence in the protrusion ÷ [integrated fluorescence in protrusion + integrated fluorescence in the rest of the cell].

Protein preparation

For the pyrene assay, *C. elegans* VCA(WSP-1/N-WASP) domain (amino acids 485-607) and VCA(WVE-1/WAVE) domain (amino acids 389-468) were cloned into pGEX4T1 with a GST tag at the N-terminus. A 8-His tag was added at the C-terminus. Proteins were purified as in (24), but with a few modifications. Briefly *C. elegans* proteins were expressed in BL21-CodonPlus(DE3)-RIPL (Stratagene) overnight at 30°C with 0.5 mM isopropyl-β-d-thiogalactoside (IPTG) in 2YT medium containing 50 μg/μl ampicillin and 17 μg/μl chloramphenicol. Cells were lysed in PBS supplemented with complete EDTA-free protease inhibitor cocktail (Roche) then purified using glutathione Sepharose (GE Healthcare). Proteins were eluted with PBS, 25 mM reduced glutathione and then supplemented to 30 mM imidazole. Proteins were bound to a Ni Sepharose High Performance column (GE Healthcare) and eluted in PBS/250 mM imidazole. Proteins were further purified over a Superdex 200 10/300GL column (GE Healthcare) in 20 mM Tris, pH 8.0, 200 mM NaCl, 0.5 mM ETDA, and 1 mM DTT. Proteins were dialyzed into 20 mM Tris, pH 8.0, 200 mM NaCl, 0.5 mM ETDA, 1 mM DTT and 10% glycerol, and stored at −80°C.

Pyrene assay

Porcine Arp2/3 complex, rabbit muscle actin and pyrene actin were purchased from Cytoskeleton. Untagged human profilin was expressed in *Escherichia coli* strain Rosetta 2(DE3) pLysS (Novagen) and purified as in (30). The pyrene assay was performed at 4 μM

actin with 5% pyrene label, 12 μM profilin, 50 nM Arp2/3 complex and the indicated amounts of VCA in a buffer containing 9 mM HEPES, 1.3 mM ATP, 2.6 mM DTT, 1.3 mM $MgCl_2$, 0.9 mM EGTA, 44 mM KCl, 1% BSA, pH 7.5. The concentration of barbed ends was calculated with the equation: [b.e.] = (Elongation rate μM/s)/(k_+ · [actin monomers]), where elongation rate at half-maximum was converted from a.u. to μM based on the curve plateau assuming all actin was in filamentous form at this point, using 2 μM as the actin monomer concentration at half-max and taking k_+ as approximately 10 $\mu M^{-1}s^{-1}$ (31, 32).

RESOLFT microscopy

Point scanning RESOLFT imaging was carried out using a custom-built setup. The setup was built around a Leica DMI 6000 microscope with a HCX PL 63x Glyc objective, lens NA 1.3 (Leica, Wetzlar, Germany). The RESOLFT illumination scheme required three modulable light sources: on-switching (405 nm), off-switching (488 nm) and read-out (488 nm) (06-MLD, Cobolt AB, Solna, Sweden). The off-switching laser passed through a vortex phase plate (VPP-1, RPC Photonics, NY, USA), which created the donut shaped beam needed for generating the sub-diffraction spatial confinement. The on-switching and the read-out beams were Gaussian shaped. The 488 nm laser lines were combined with a polarizing beam splitter (B. Halle, Berlin, Germany) and then the 488 and 405 using a 458 long pass filter (ZT458rdc, Chroma Technology, VT, USA). A set of galvo mirrors (6215HSM40B, Cambridge Technology, MA, USA) where used for xy scanning. The stage had built-in z piezo (PI, Karlsruhe, Germany). The stage was mounted directly onto the objective lens in order to minimize drift and vibration. The emission light was separated from the laser light using a 488 LP filter (ZT488rdc, Chroma, VT, USA) and further passed through a 535 BP filter (E535/70M, Chroma, VT, USA) before being collected by a SPAD (MPD, Bolzano, Italy). For time-lapse acquisitions, the minimum time between z-stacks was 1.5 minutes. The hardware was controlled using custom designed software based on LabVIEW and National Instrument's FPGA (NI, TX, USA). The RESOLFT images were deconvolved using a Richard and Lucy algorithm, with 2 iterations and a PSF width of 80 nm. All the imaging was performed with illumination intensities on the order of 3 KW/cm^2 for on-switching, 9 KW/cm^2 for off-switching and 12 KW/cm^2 for read-out of the fluorescence signal.

Supplemental Figures

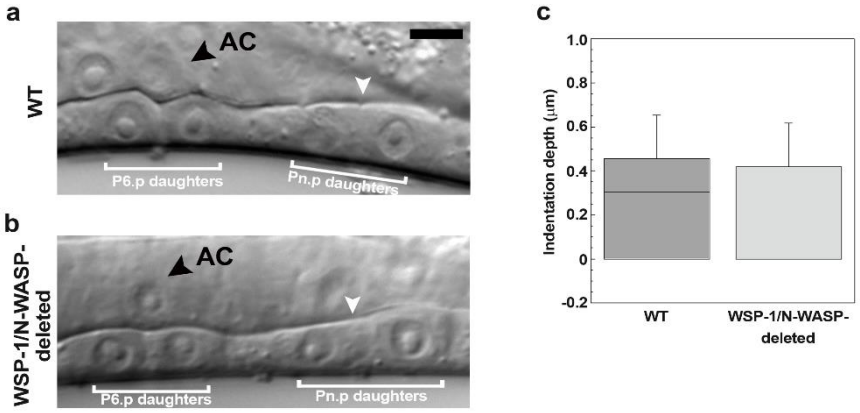

Supplemental Figure S1 BM deformations over Pn.p daughter cells. To show that BM indentation is specific to the AC, the depth of indentation over the P5.p and P7.p daughter cell-pairs on either side of the AC is evaluated. **(a)** and **(b)** representative images of the P6.p daughter cells under the AC and the adjacent Pn.p daughter cells in WT and WSP-1/N-WASP-deleted worms, respectively. The AC is indicated by black arrowheads and the white arrowheads indicate where the indentation measurement was taken between pairs of Pn.p daughters. Only one pair of Pn.p descendants is shown here for each condition, although daughters of both adjacent Pn.p cells (P5.p and P7.p) were often analyzable. **(c)** Quantification of depth of deformation over Pn.p daughter cells in WT and WSP-1/N-WASP-deleted worms. Compared to indentations over P6.p daughters (Figure 1d), Pn.p daughters are significantly less indented in both WT and WSP-1/N-WASP-deleted animals: for WT Pn.p indentation depth is 0.3 ± 0.3 μm ($p < 0.0001$ as compared to P6.p) and for WSP-1/N-WASP-deleted animals, indentation depth is 0.2 ± 0.2 μm ($p = 0.0005$ as compared to P6.p) indicating an AC-specific effect. The BM was often, but not always, flat over Pn.p daughter cells. $N \geq 9$ for each condition. DIC microscopy. Bar 5 μm.

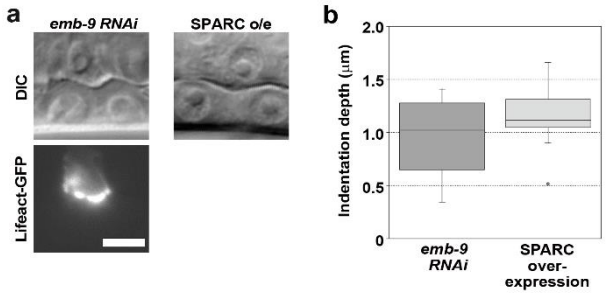

Supplemental Figure S2 Weakening BM does not increase indentation depth.

BM is weakened by either *emb-9* RNAi or SPARC overexpression, and worms are examined at the P6.p 2-cell stage. **(a)** Representative images. **(b)** No differences in indentation depth are observed as compared to WT (Figure 1c and d): average indentation depths are 1.0 ± 0.3 μm for *emb-9* RNAi treatment ($p = 0.2$ compared with WT) and 1.2 ± 0.3 μm for SPARC overexpression worms ($p = 0.6$ compared with WT). $N \geq 13$. SPARC overexpression is verified by GFP presence, and efficiency of *emb-9* RNAi is confirmed by observing almost complete adult rupture and death. Epifluorescence microscopy. Bar 5 μm.

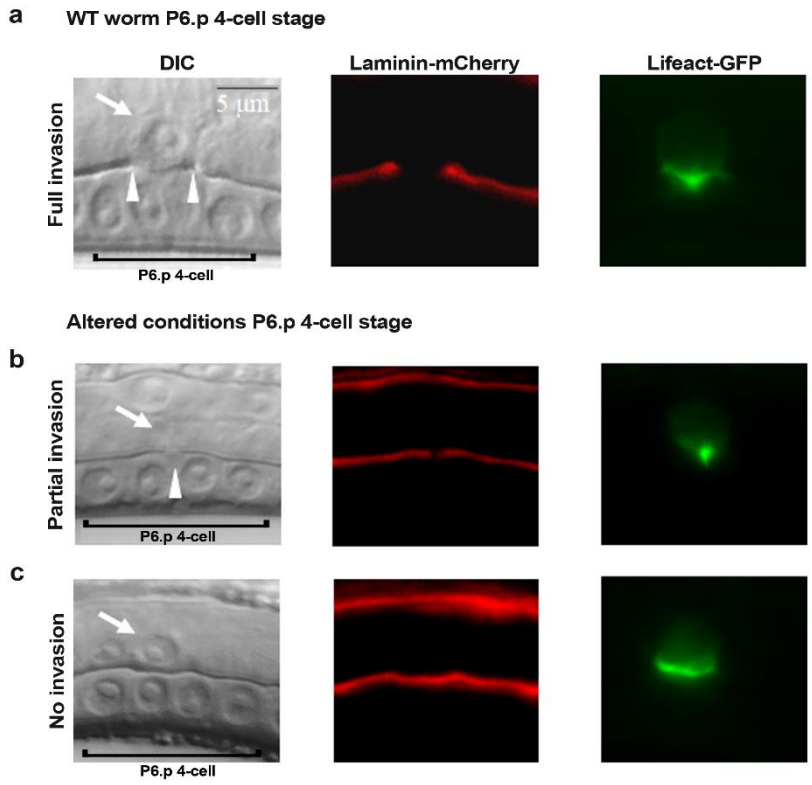

Supplemental Figure S3 AC invasion scoring. (a) At the P6.p 4-cell, the AC (arrow) in WT worms has completely cleared the underlying BM (arrowheads mark the edges of the BM hole). The hole is also clear in the fluorescent image of the BM (*Plam-1::laminin::mCherry*), and AC F-actin (*Pcdh-3::Lifeact::GFP*) fills the gap. In conditions where invasion is perturbed, effacement of the BM at the 4-cell stage can be either partial **(b)** or non-existent **(c)**. The images shown are of the *wsp-1 (gm324)* mutant crossed into the *qyIs127[Plam-1::laminin::mCherry]; qyIs242 [Pcdh-3::Lifeact::GFP]* background. In **(b)**, the AC (arrow) makes a small hole in the BM (arrowhead), corresponding to a small gap in the laminin fluorescence and a small F-actin protrusion. In **(c)**, when invasion is completely blocked, the BM line remains intact beneath the AC (arrow) as observed by DIC, no breaks are evident in the laminin channel and the actin region is flat. In practice, most scoring is done using DIC images as shown on the left, and the number of worms in each category is counted for a given treatment. Epifluorescence microscopy. Bar 5 µm.

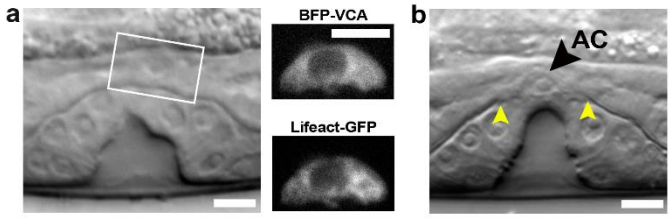

Supplemental Figure S4 Complete failure of VCA-expressing AC to invade.

(a) When VCA is expressed in the AC, the AC fails to invade even at the P6.p 8-cell stage, and the BM (visualized as a phase dense line) remains intact in 90% of animals (N = 40), unlike in WT at the same stage **(b)**, where the BM gap is indicated (yellow arrowheads). Spinning disc microscopy. All bars 5 μm.

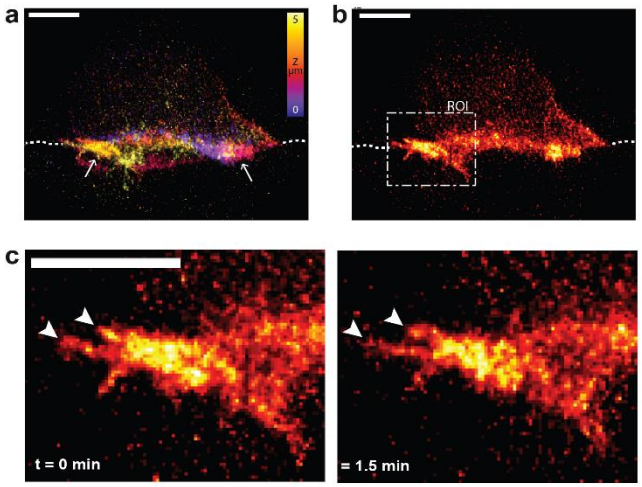

Supplemental Figure S5 AC invasive protrusion is very dense as observed by RESOLFT super-resolution microscopy (a)-(c) Actin is visualized by RESOLFT super-resolution microscopy using a worm strain expressing in the AC the reversible, photoswitchable fluorescent protein DronpaM159T fused to Lifeact (*Pcdh-3::Dronpa::Lifeact*). **(a)** A representative AC volume, in which the colors represent different depths, from 0 to 5 µm (see inset). Dense structures are observed at the invasive membrane (arrows), and the individual fibers are unresolvable in these patches. Patches span several µm in both x and z direction. **(b)** A maximum intensity projection of the three center planes of the volume shows fine branched structures on the protrusion edge (box labeled ROI). **(c)** Two frames of a time-lapse sequence taken of the ROI in **(b)**. The fine actin structures visible on the edges of the invasive protrusion (arrowheads) appear to be filament bundles as they have widths in the range of 80-120 nm. Comparing the two images taken over time reveal that these actin fingers are growing laterally as regards the BM plane (represented by dotted lines in **(a)** and **(b)**), perhaps helping to push open the BM hole. Scale bars are 2 µm.

a

Background (genotype)	RhoGTPase RNAi treatment	% Full invasion	% Partial invasion	% No invasion	N	
cdc-42(gk388)	*cdc-42*[a]	68	8	24	25	
mig-2 (mu28)[b]	--	100	0	0	54	
ced-10(tm597)	*ced-10*	97	3	0	42	
wsp-1 (gm324)[c]	--	18	21	61	34	#
wsp-1 (gm324)	*cdc-42*	20	17	63	41	#
wsp-1 (gm324)	*mig-2*	17	14	69	66	**
wsp-1 (gm324)	*ced-10*	5	23	72	56	
wve-1 (ne350)[c]	--	94	3	3	35	#
wve-1 (ne350)	*ced-10*	96	0	4	55	
wve-1 (ne350)	*mig-2*	90	6	4	49	
wve-1 (ne350)	*cdc-42*	81	11	8	37	
mig-2 (mu28)	*cdc-42*	21	15	64	53	
mig-2 (mu28)	*ced-10*	58	24	18	59	

b

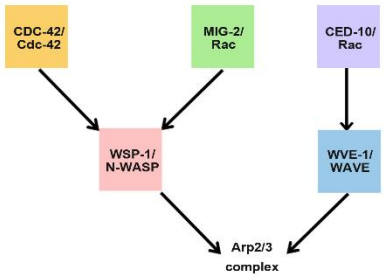

[a] Data from supplemental reference (12).
[b] Data from supplemental reference (20).
[c] Data taken from Supplemental Table 1 for comparison.
not significant p > 0.05
**significant p = 0.05

Supplemental Figure S6 Cooperation between WSP-1/N-WASP and WVE-1/WAVE is reflected in the roles of upstream RhoGTPases. (a) The Rho GTPases CDC-42/Cdc-42 (yellow), MIG-2/Rac (green) and CED-10/Rac (purple) are knocked-down in WSP-1/N-WASP (pink), WVE-1/WAVE (blue) and MIG-2/Rac (green) mutant backgrounds. AC invasion is evaluated at the P6.p 4-cell stage and full, partial and no invasion events are counted, for a total number of worms N for each condition. Significance tests are performed on the % full invasion data for the comparison of selected conditions. See also Supplemental Results and Discussion. Where indicated, data was taken from previous publications. **(b)** Scheme summarizing how RhoGTPases interact with WSP-1/N-WASP and WVE-1/WAVE.

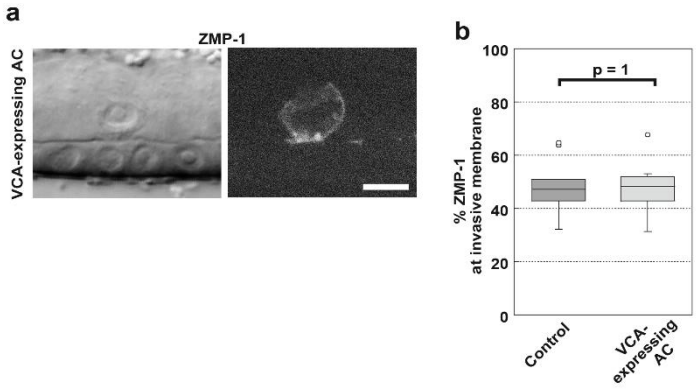

Supplemental Figure S7 VCA expression in the AC completely blocks invasion, but does not perturb ZMP-1 localization. (a) Representative images of ZMP-1 localization (GFP-ZMP-1-GDI) in VCA-expressing AC. Single plane images of worms at the P6.p 4-cell stage. **(b)** Quantification of the % of the total fluorescent signal found at the invasive membrane for ZMP-1 (see Supplemental Methods) with control data reproduced from Figure 3f for comparison. $N \geq 7$. Spinning disc microscopy. Bar 5 μm.

Supplemental Video Legends

Supplemental Video S1 WT invasion with F-actin visualized by Lifeact-GFP. The still images of **Figure 2a** are taken from this movie, and the movie spans the entire curve shown in **2c**, green curve. Maximum intensity projection of z-stacks. Spinning disc microscopy. Movie in real time spans 71 minutes. Acceleration is approximately 600x. Bar 5 μm.

Supplemental Video S2 Mutant invasion in the absence of WSP-1/N-WASP with F-actin visualized by Lifeact-GFP. The still images of **Figure 2b** are taken from this movie, and the movie spans the entire curve shown in **2c**, orange curve. Maximum intensity projection of z-stacks. Spinning disc microscopy. Movie in real time spans 57 minutes. Acceleration is approximately 600x. Bar 5 μm.

References for Supplemental Results and Discussion, Table, Methods and Figures

1. Walck-Shannon E, Reiner DJ, & Hardin J (2015) Polarized Rac-dependent protrusions drive epithelial intercalation in the embryonic epidermis of *C. elegans*. Development 142:3549-3560.
2. Lundquist EA, Reddien PW, Hartwieg E, Horvitz HR, & Bargmann CI (2001) Three *C. elegans* Rac proteins and several alternative Rac regulators control axon guidance, cell migration and apoptotic cell phagocytosis. Development 128:4475-4488.
3. Reiner DJ & Lundquist EA (2016) Small GTPases. Wormbook:1-99.
4. Shakir MA, Jiang K, Struckhoff EC, Demarco RS, Patel FB, Soto MC, & Lundquist EA (2008) The Arp2/3 activators WAVE and WASP have distinct genetic interactions with Rac GTPases in Caenorhabditis elegans axon guidance. Genetics 179:1957-1971.
5. Patel FB, Bernadskaya YY, Chen E, Jobanputra A, Pooladi Z, Freeman KL, Gally C, Mohler WA, & Soto MC (2008) The WAVE/SCAR complex promotes polarized cell movements and actin enrichment in epithelia during C. elegans embryogenesis. Dev. Biol. 324:297-309.
6. Soto MC, Qadota H, Kasuya K, Inoue M, Tsuboi D, Mello CC, & Kaibuchi K (2002) The GEX-2 and GEX-3 proteins are required for tissue morphogenesis and cell migrations in *C. elegans*. Genes Dev. 16:620-632.
7. Mi-Mi L, Votra S, Kemphues K, Bretscher A, & Pruyne D (2012) Z-line formins promote contractile lattice growth and maintenance in striated muscles of *C. elegans*. J. Cell Biol. 198:87-102.
8. Sawa M, Suetsugu S, Sugimoto A, Miki H, Yamamoto M, & Takenawa T (2003) Essential role of the *C.elegans* Arp2/3 complex in cell migration during ventral enclosure. J. Cell Sci. 116:1505-1518.
9. Moulder GL, Cremona GH, Duerr J, Stirman JN, Fields SD, Martin W, Qadota H, Benian GM, Lu H, & Barstead RJ (2010) α-actinin is required for proper assembly of Z-disk / focal adhesion-like structures and for efficient locomotion in Caenorhabditis elegans. J. Mol. Biol. 403:516-528.
10. DeMaso CR, Kovacevic I, Uzun A, & Cram EJ (2011) Structural and functional evaluation of C. elegans filamins FLN-1 and FLN-2. PLOS One 6:e22428.
11. Ding WY, Ong HT, Hara Y, Wongsantichon J, Toyama Y, Robinson RC, Nédélec F, & Zaidel-Bar R (2017) Plastin increases cortical connectivity to facilitate robust polarization and timely cytokinesis. J. Cell Biol. 216:1371-1386.
12. Lohmer LL, Clay MR, Naegeli KM, Chi Q, Ziel JW, Hagedorn EJ, Park JE, Jayadev R, & Sherwood DR (2016) A sensitized screen for genes promoting invadopodia function in vivo: CDC-42 and Rab GDI-1 direct distinct aspects of invadopodia formation. PLOS Genetics 12(1):e1005786.
13. Withee J, Galligan B, Hawkins N, & Garriga G (2004) *Caenorhabditis elegans* WASP and Ena/VASP protiens play compensatory roles in morphogenesis and neuronal cell migration. Genetics 167:1165-1176.
14. Matus DQ, Lohmer LL, Kelley LC, Schindler AJ, Kohrman AQ, Barkoulas M, Zhang W, Chi Q, & Sherwood DR (2015) Invasive cell fate requires G1 cell-cycle arrest and histone deacetylase-mediated changes in gene expression. Dev. Cell 35:162-174.
15. Kovacevic I & Cram EJ (2010) FLN-1/Filamin is required for maintenance of actin and exit of fertilized oocytes from the spermatheca in *C. elegans*. Dev. Biol. 347:247-257.
16. Shaye DD & Greenwald I (2016) A network of conserved formins, regulated by the guanine exchange factor EXC-5 and the GTPase CDC-42, modulates tubulogenesis *in vivo*. Development 143:4173-4181.
17. Zhu Z, Chai Y, Jiang Y, Li W, Hu H, Li W, Wu J-W, Wang Z-Z, Huang S, & Ou G (2016) Functional coordination of WAVE and WASP in *C. elegans* neuroblast migration. Dev. Cell 39:224-238.
18. Hagedorn EJ, Ziel JW, Morrissey MA, Linden LM, Wang Z, Chi Q, Johnson SA, & Sherwood DR (2013) The netrin receptor DCC focuses invadopodia-driven basement membrane transmigration in vivo. J. Cell Biol. 201:903-913.

19. Ihara S, Hagedorn EJ, Morrissey MA, Chi Q, Motegi F, Kramer JM, & Sherwood DR (2011) Basement membrane sliding and targeted adhesion remodels tissue boundaries during uterine vulval attachment in Caenorhabditis elegans. Nat. Cell Biol. 13:641-651.
20. Ziel JW, Hagedorn EJ, Audhyu A, & Sherwood DR (2009) UNC-6 (netrin) orients the invasive membrane of the anchor cell in *C. elegans*. Nat. Cell Biol. 11:183-189.
21. Naegeli KM, Hastie EL, Garde A, Wang Z, Keeley DP, Gordon KL, Pani AM, Kelley LC, Morrissey MA, Chi Q, Goldstein B, & Sherwood DR (2017) Cell invasion in vivo via rapid exocytosis of a transient lysosome-derived membrane domain. Dev. Cell 43:403-417.
22. Morrissey MA, Jayadev R, Miley GR, Blebea CA, Chi Q, Ihara S, & Sherwood DR (2016) SPARC promotes cell invasion in vivo by decreasing type IV collagen levels in the basement membrane. PLOS Genet. 12:e1005905.
23. Hagedorn EJ, Yashiro H, Ziel JW, Ihara S, Wang Z, & Sherwood DR (2009) Integrin Acts Upstream of Netrin Signaling to Regulate Formation of the Anchor Cell's Invasive Membrane in C. elegans. Dev. Cell 17:187-198.
24. Havrylenko S, Noguera P, Abou-Ghali M, Manzi J, Faqir F, Lamora A, Guérin C, Blanchoin L, & Plastino J (2015) WAVE binds Ena/VASP for enhanced Arp2/3 complex-based actin assembly. Mol. Biol. Cell 26:55-65.
25. Kaucikas M, Tros M, & van Thor JJ (2015) Photoisomerization and proton transfer in the forward and reverse photoswitching of the fast-switching M159T mutant of the Dronpa fluorescent protein. J. Phys. Chem B 119:2350-2362.
26. Redemann S, Schloissnig S, Ernst S, Pozniakowsky A, Ayloo S, Hyman AA, & Bringmann H (2011) Codon adaptation–based control of protein expression in *C. elegans*. Nat. Meth. 8:250-252.
27. Morrissey MA, Keeley DP, Hagedorn EJ, McClatchey STH, Chi Q, Hall DH, & Sherwood DR (2014) B-LINK: a hemicentin, plakin, and integrin-dependent adhesion system that links tissues by connecting adjacent basement membranes. Dev. Cell 31:319-331.
28. Rual JF, Ceron J, Koreth J, Hao T, Nicot AS, Hirozane-Kishikawa T, Vandenhaute J, Orkin SH, Hill DE, van den Heuvel S, & Vidal M (2004) Toward improving *Caenorhabditis elegans* phenome mapping with an ORFeome-based RNAi library. Genome Res. 14:2162-2168.
29. Kelley LC, Wang Z, Hagedorn EJ, Wang L, Shen W, Lei S, Johnson SA, & Sherwood DR (2017) Live-cell confocal microscopy and quantitative 4D image analysis of anchor-cell invasion through the basement membrane in *Caenorhabditis elegans*. Nat. Protoc. 10:2081-2096.
30. Carvalho K, Lemière J, Faqir F, Manzi J, Blanchoin L, Plastino J, Betz T, & Sykes C (2013) Actin polymerization or myosin contraction: two ways to build up cortical tension for symmetry breaking. Phil. Trans. R. Soc. B 368:20130005.
31. Higgs HN, Blanchoin L, & Pollard TD (1999) Influence of the C terminus of Wiskott-Aldrich syndrome protein (WASp) and the Arp2/3 complex on actin polymerization. Biochemistry 38(46):15212-15222.
32. Pollard TD (1986) Rate constants for the reactions of ATP- and ADP-actin with the ends of actin filaments. J. Cell Biol. 103:2747-2754.